J. Astrophys. Astr. (2020) 41:33
https://doi.org/10.1007/s12036-020-09652-9

REVIEW

Observations with the 3.6-meter Devasthal optical telescope

RAM SAGAR[1,2,*], BRIJESH KUMAR[2] and SAURABH SHARMA[2]

[1]Indian Institute of Astrophysics, Sarjapur Road, Koramangala, Bengaluru 560 034, India.
[2]Aryabhatta Research Institute of Observational Sciences, Manora Peak, Nainital 263 001, India.
E-mail: ramsagar@iiap.res.in

MS received 20 August 2020; accepted 5 October 2020

Abstract. The 3.6-meter Indo–Belgian Devasthal optical telescope (DOT) has been used for optical and near-infrared (NIR) observations of celestial objects. The telescope has detected stars of $B = 24.5 \pm 0.2, R = 24.6 \pm 0.12$ and $g = 25.2 \pm 0.2$ mag in exposure times of 1200, 4320 and 3600 s respectively. In one hour of exposure time, a distant galaxy of 24.3 ± 0.2 mag and point sources of ~ 25 mag have been detected in the SDSS *i* band. The NIR observations show that stars up to $J = 20 \pm 0.1, H = 18.8 \pm 0.1$ and $K = 18.2 \pm 0.1$ mag can be detected in effective exposure times of 500, 550 and 1000 s respectively. The *nbL* band sources brighter than ~ 9.2 mag and strong (≥ 0.4 Jy) *PAH* emitting sources like Sh 2-61 can also be observed with the 3.6-meter DOT. A binary star with angular separation of $0.''4$ has been resolved by the telescope. Sky images with sub-arcsec angular resolutions are observed with the telescope at wavelengths ranging from optical to NIR for a good fraction of observing time. The on-site performance of the telescope is found to be at par with the performance of other, similar telescopes located elsewhere in the world. Owing to the advantage of its geographical location, the 3.6-meter DOT can provide optical and NIR observations for a number of frontline galactic and extra-galactic astrophysical research problems, including optical follow-up of GMRT and AstroSat sources and optical transient objects.

Keywords. Optical telescope—Sky performance—Detection limits at optical and near-infrared wavelengths.

1. Introduction

Devasthal (meaning abode of God) is a mountain peak (longitude 79.° 7 E, latitude 29.° 4 N, and altitude 2424 ± 4 m). It is located at a distance of ∼55 km by road from Nainital in Kumaon region of central Himalaya. Figure 1 shows an aerial view of the Devasthal observatory and a topographic contour map of the region. The location was identified after decades of detailed site survey using modern instruments (Sagar 2000; Stalin 2001 and references therein). After successful installation and technical checks the 3.6-meter Indo–Belgian Devasthal optical telescope (DOT) was activated by the prime ministers of India and Belgium from Brussels on March 30, 2016, and since then it is in use for training people, testing back-end instruments, and making observations of various types of celestial objects.

A description of the actively supported and modern DOT is given in the next section. Back-end instruments presently in use and results of sky performance derived from the optical and near-infrared (NIR) observations made with the telescope are given in the remaining sections. The last section provides a summary and future outlook for this international observing facility.

2. The 3.6-meter DOT

The modern, actively supported 3.6-meter DOT is an f/9 two-mirror Ritchey–Chrétien system. It has three Cassegrain ports with a back focal distance of 2.5 m. Details

This article is part of the Topical Collection: Chemical elements in the Universe: Origin and evolution.

Published online: 11 December 2020

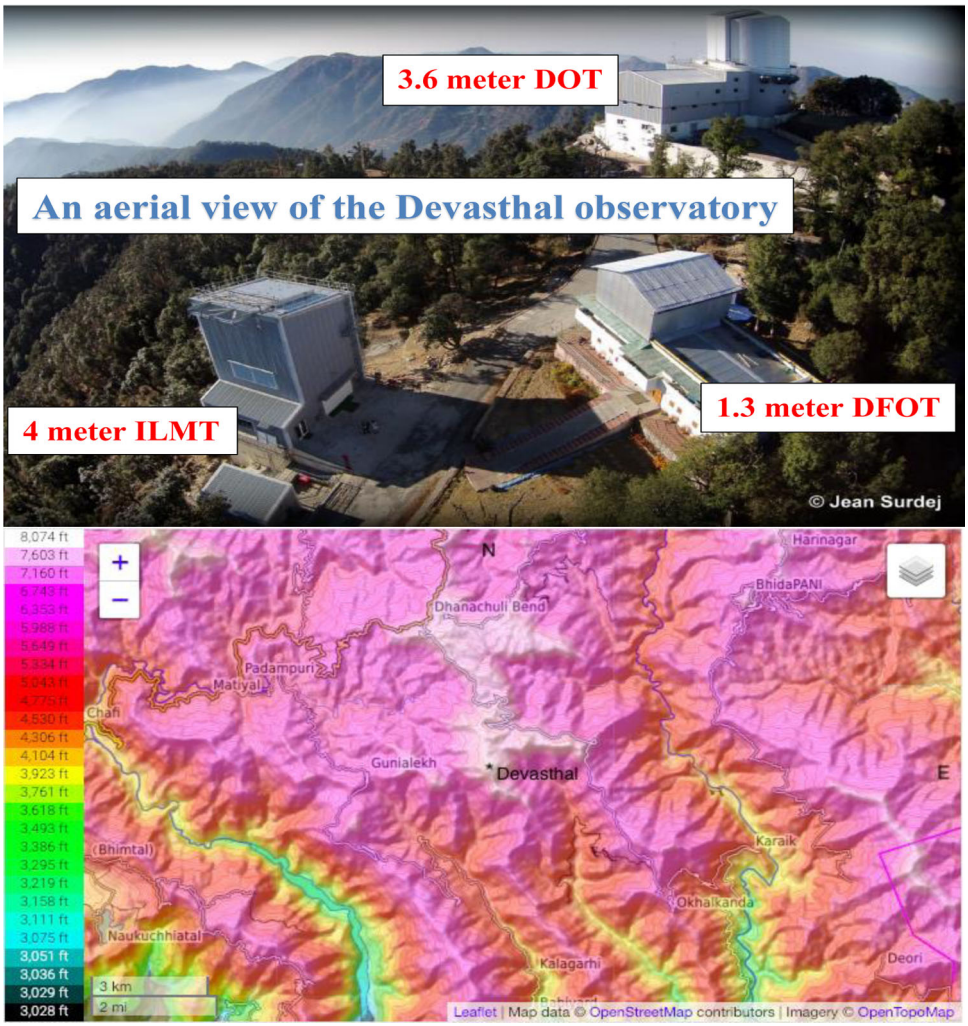

Figure 1. The lower part shows the topographic contour map of Devasthal and its immediate surroundings. North is up and East is to the right in this map. Devasthal, the highest peak in the region of ≥ 10 km range, is at a point which has sharp altitude gradient towards the south-west, the prevailing incoming wind direction at the site. This location is therefore expected to provide laminar air flow, resulting in better seeing for astronomical observations. An aerial view of the Devasthal Observatory is shown in the upper part. The buildings housing the 3.6-meter DOT, 1.3-meter Devasthal fast optical telescope (DFOT) (Sagar *et al.* 2011) and 4-meter International Liquid Mirror Telescope (ILMT) (Surdej *et al.* 2018) are marked. Source: Ram Sagar, *Resonance*, Vol 25, No. 11, pp. 1507–1526, 2020

of history, technical aspects, construction of building, mirror coating, installation of the telescope, etc. are given in Omar *et al.* (2017), Kumar *et al.* (2018), Omar *et al.* (2019c) and Sagar *et al.* (2019a) along with a few initial scientific results. To detect and correct deformations, aberrations, or any other phenomena that degrade the image quality of the telescope, the 3.6-meter DOT is equipped with an active optics system (AOS) which compensates for distorting forces that change relatively slowly, roughly on timescales of seconds. The AOS consists of a wave front sensor (WFS), primary (M1) mirror support system consisting of 69 actuators generating forces on M1 mirror and three axial definers with load cells on M1 mirror, secondary (M2) mirror hexapod that supports M2 mirror, and the telescope control system (TCS) which acts as interface between the elements of the telescope. Manufacturing surface inaccuracies of mirrors and imperfection in integration of the mirrors in their cells, gravity load, thermal effects and wind effects are the main sources of telescope image degradation. A WFS is used to measure and analyze the wave front coming from the telescope system. Its output is used to improve telescope image. Astigmatism, 3-fold and spherical aberration are corrected with the actuators of M1 mirror support, while focus, coma and tilt can be corrected with the M2 mirror hexapod. Load cells measure the residual forces on the three axial definers and the actuators are used to keep these forces zero. The

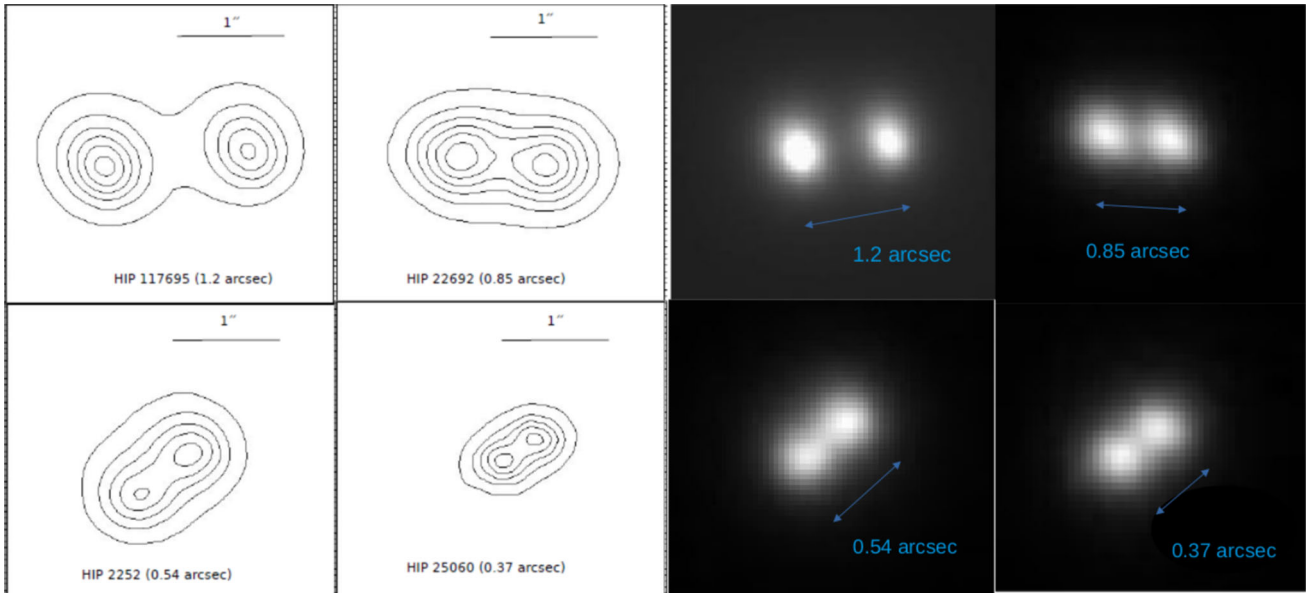

Figure 2. The Iso-intensity contours and images of four binary stars are shown. The images of binary stars with known angular separation between 0.″37 and 1.″2 were taken with the test camera mounted at the axial Cassegrain port of 3.6-meter DOT. The image shows that the binary star with angular separation of 0.″37 is well resolved.

repeatable corrections on M1 and M2 mirrors are applied in open-loop mode (look-up table), whereas the closed-loop mode applies both repeatable and non-repeatable corrections. The latter arises from thermal deformations and wind effects. The telescope uses sophisticated and complex techniques for achieving and maintaining image quality while tracking objects in the sky. DOT thus has online optics alignment while taking images of celestial objects and differs from classical telescopes where AOS is not used.

TCS accepts coordinates of both target and the guide star. Acting as the interface between the hardware of the telescope and the user, TCS provides access to both the operational and engineering control of the telescope hardware. It also interfaces with AOS, guiding unit system and the back-end instruments. Further details on this are given in Kumar *et al.*(2018) and Sagar *et al.* (2019a).

2.1 *Imaging of close binaries*

During commissioning, a test camera, an air-cooled Microline ML 402ME CCD chip of 768 × 512 pixels, was used to quantify performance of the 3.6-meter DOT. It has a pixel size of 9 μm which corresponds to 0.″06 at the focal plane of the telescope. During November-December 2015, the test camera imaged a few binary stars of known angular separation in broadband (0.45 to 0.6 μm) visual glass filter. These images revealed that binary stars having sub-arcsec separation are clearly resolved (Figure 2). The best angular resolution of $\sim$0.″4 was achieved on the night of 30 November 2015. More information on these observations are given in Kumar *et al.* (2018),

2.2 *Allotment of observing time*

Observing proposals from users are submitted online twice in a year for both observing cycles, namely cycle-1 (February to May) and cycle-2 (October to January). The website[1] provides relevant information regarding the policies and procedures followed in allotment of observing time for the telescope. Based on scientific merit of the submitted proposals, the Belgian and Indian time allocation committees allot observing time to the proposers of their countries. Presently, 33% and 7% observing time are allotted to proposers from ARIES and Belgium respectively, while the remaining 60% observing time is allotted to other proposers. Updated information on existing back-end instruments on the 3.6-meter DOT is given below.

3. Cassegrain port instruments

The telescope has capacity to bear imbalance of 2000 Nm on altitude axes and of 400 Nm on azimuth axes. Imbalances are adjustable using motorized weights on

[1] https://www.aries.res.in.

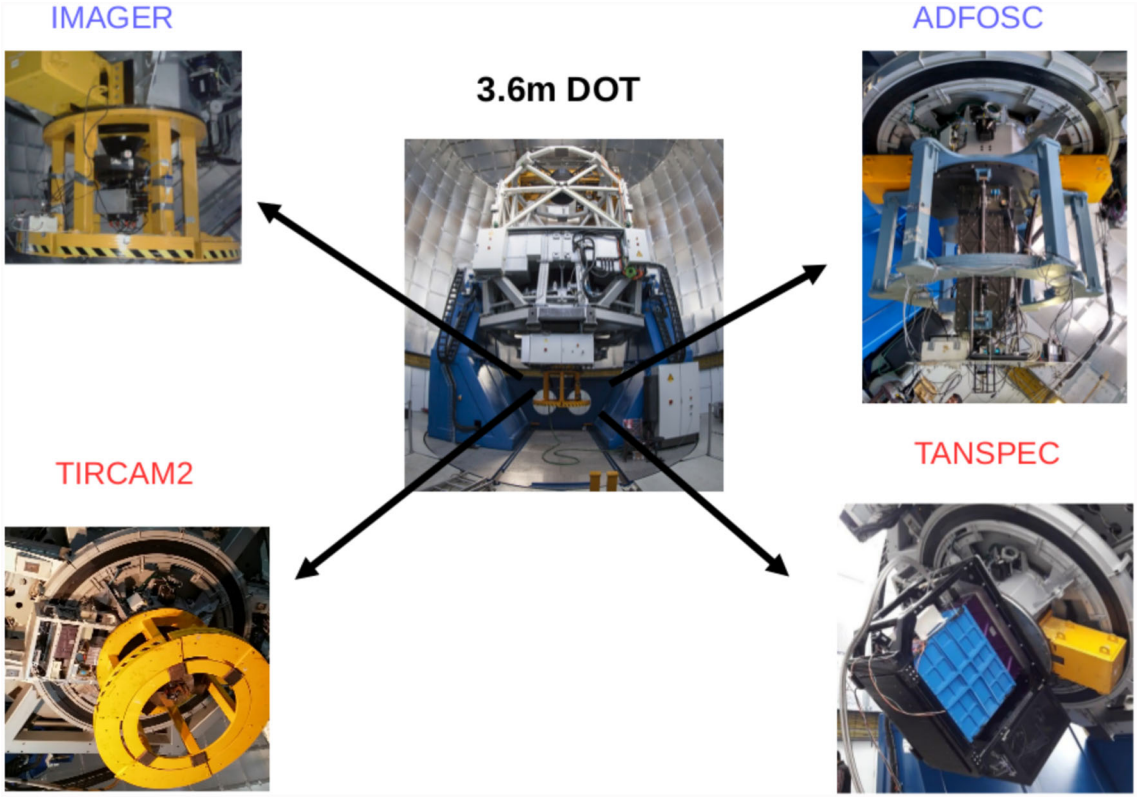

Figure 3. The 3.6-meter DOT is in the center. The other pictures show back-end instruments 4K × 4K CCD IMAGER, ADFOSC, TIRCAM2 and TANSPEC used for regular observations.

altitude axes and fixed weights on azimuth axes. There are three Cassegrain ports available for mounting back-end instruments on the 3.6-meter DOT. The main axial port is designed for mounting instruments weighing up to 2000 kg. The telescope interface plate (TIP) is used for mounting axial-port instrument. Sagar *et al.* (2019a) has a detailed description of the shape and dimensions of TIP. The center of gravity (CG) of axial-port instrument is 80 cm below TIP. A one-cm shift of CG on the vertical axis creates a torque of 200 Nm. This value is very close to the altitude bearing friction. Hence, mounting of any axial-port instrument needs careful adjustment of its CG. The side-port instruments can have a weight of 250 kg each with CG 62 cm away from the centre of TIP. The main axial and two side instrument ports are fixed to a structure called ARISS. The device which rotates the image of the sky and side-port fold mirror are also part of ARISS. All these units are nested at the rear of M1 mirror. Figure 3 shows pictures of the telescope along with back-end instruments presently in use for regular observations. IMAGER and ADFOSC (ARIES-Devasthal Faint Object Spectrograph and Camera) are used in optical region while TIRCAM2 (TIFR NIR Imaging Camera-II) and TANSPEC (TIFR-ARIES NIR Spectrometer) are used in NIR region. The 3.6-meter DOT has been used for detailed characterization of these instruments as well as for observations of science proposals related to photometric and spectroscopic study of galactic star-forming regions, star clusters, AGNs and quasars, supernovae, optical transient events, distant galaxies, etc. The following subsections provide technical details of these back-end instruments.

3.1 *IMAGER: Optical imaging camera*

IMAGER, with wavelength sensitivity between 0.35 μm and 0.9 μm, has been indigenously designed, developed and assembled at ARIES. Pandey *et al.* (2018) provides technical details of optical and mechanical design, motorized filter wheels and data acquisition system of the instrument. The pixel size of a blue-enhanced liquid nitrogen cooled ($\sim -120^{\circ}$) STA4150 4K × 4K CCD sensor is 15 μm square. Standard broadband Bessel U, B, V, R and I, and SDSS u, g, r, i and z filters are presently mounted. The

field of view (FOV) of IMAGER is $6.'5 \times 6.'5$ at the Cassegrain focus of the telescope. IMAGER has been used extensively for taking images of both point and extended sources in the sky.

3.2 *ADFOSC: Optical imaging and spectroscopic camera*

ADFOSC is a low-resolution slit-spectrograph-cum-imager with wavelength sensitivity between 0.35 μm and 0.9 μm. This instrument also has been designed, developed and assembled in-house at ARIES. Omar *et al.* (2019a, b, c) provides its detailed technical parameters along with its performance. Briefly, a collimator and a focal reducer are used to convert the telescope f/9 beam to an ADFOSC f/4.3 beam. The detector used is a closed-cycle, cryogenically cooled grade-0 back-illuminated E2V 231-84 chip of a 4096×4096 square-pixel CCD camera. ADFOSC can be used in three modes of observations named (a) broadband and narrowband photometric imaging, (b) long-slit low-resolution ($\lambda/\Delta\lambda \sim 1000$) and slitless spectroscopy, and (c) fast imaging (up to millisecond cadence) using an electron-multiplier frame-transfer CCD with smaller FOV and on-chip binning. In photometric imaging mode, it is equipped with SDSS *u*, *g*, *r*, *i* and *z* filters, 8′-long slits, grisms, and narrow-band filters, and can image a FOV of $13.'6 \times 13.'6$ when mounted on the telescope. It has been used in both imaging and spectroscopy modes for observations of stars, ionized star-forming regions, galaxies, etc. (Omar *et al.* 2019a, b).

3.3 *TIRCAM2: NIR imaging camera*

TIRCAM2, developed by Tata Institute of Fundamental Research (TIFR) (Naik *et al.* 2012), is a closed-cycle helium cryo-cooled imaging camera equipped with a Raytheon 512×512 pixels InSb Aladdin III quadrant focal plane array. This imaging camera has sensitivity from $\lambda = 1$ μm to $\lambda = 3.7$ μm. Pixel scale of the camera on the telescope is $0.''17$ with a FOV of $86.''5 \times 86.''5$. TIRCAM2 was mounted on the axial port of the telescope for tests, characterization and science observations. Further details of this camera are given in Ojha *et al.* (2018) and Baug *et al.* (2018). It is equipped with standard *J* (1.2 μm), *H* (1.65 μm) and *K* (2.19 μm) broad ($\Delta\lambda \sim 0.3$–0.4 μm) photometric bands, and narrow ($\Delta\lambda \sim 0.03$–0.07 μm) band $B_{r-\gamma}$ (2.16 μm), $K_{\rm cont}$ (2.17 μm), polycyclic aromatic hydrocarbon (PAH) (3.29 μm), and narrowband L (*nbL*) (3.59 μm) filters. TIRCAM2 provides sampling time of ~ 256 ms for the full frame and ~ 16 ms for a sub-array window of 32×32 square pixels. TIRCAM2 is being used for deep NIR imaging of celestial sources as well as for fast imaging in case of lunar/planet occultation events. Because of its observational capability of up to 3.59 μm, this camera is an extremely valuable instrument for observing those bright nbL and PAH sources which are saturated in the Spitzer Infrared Array Camera observations.

3.4 *TANSPEC: Optical-NIR imaging and spectroscopic camera*

TANSPEC, jointly developed by TIFR and ARIES, is an optical-NIR medium-resolution spectrograph. It covers λ from 0.55 μm in optical up to 2.54 μm in NIR, with a resolving power of ~ 2750. It can be used for simultaneous observations across entire wavelength regions. Optical layout and technical details of this instrument are provided in Ojha (2018). Briefly, it converts the f/9 telescope beam into f/12 beam on to a slit with range of widths from $0.''5$ to $4.''0$. One pixel of the spectrograph 2048×2048 Hawaii-2RG (H2RG) array corresponds to $0.''25$, and it operates in two modes. In the highest-resolution (~ 2750) mode, combination of a grating and two prisms is used, while low-resolution (~ 100–350) prism mode is used for high-throughput observations. The instrument also has an independent imaging camera with a $1K \times 1K$ H1RG detector which is the slit viewer. FOV of the slit viewer is $1' \times 1'$ while its one pixel corresponds to $0.''25$ on the sky. This camera is used for telescope guiding as well as for sky imaging. It also functions as a pupil viewer for instrument alignment on the telescope. It is equipped with both broadband (r', i', Y, J, H, Ks) and narrowband (H_2 & B_r) filters. After successful completion of laboratory tests at Mauna-Kea Infrared, USA, TANSPEC was transported to Devasthal. It was mounted and successfully tested as a back-end instrument on the 3.6-meter DOT during April-May 2019. The initial results of performance tests of TANSPEC are found to be very encouraging since they are at par with the design specifications. A detailed paper on these commissioning tests of TANSPEC is under preparation.

4. Factors affecting detection limit of a telescope

The light-gathering power of an optical telescope is related to the diameter (D) of its primary mirror that collects and focuses the light. With higher values of D, more photons are collected owing to larger areas, which makes it possible to study relatively fainter stars. For sky background limited observations (Sagar 2017), efficiency of a telescope to detect a celestial object at a frequency (ν) is $\propto \sqrt{\frac{A_{\rm eff}\times I(t)}{\epsilon_{\rm D}\times B(\nu)}}$, where $A_{\rm eff}$ is the light-gathering power of a telescope of diameter D including the losses due to optics and the quantum efficiency of the detector used at the focus of the telescope, $B(\nu)$ the sky background intensity at frequency ν, $I(t)$ the integration time, and $\epsilon_{\rm D}$ the solid angle formed by the combination of atmospheric seeing and image degradation introduced due to optical and mechanical elements of the telescope including improper focusing as discussed earlier in Section 2. The light-gathering power, $A_{\rm eff}$, of 3.6-meter DOT mainly depends on reflectivity of both M1 and M2 mirrors, the losses due to optical components, and the quantum efficiency of the detectors used in the back-end instruments. The value of sky background, $B(\nu)$, depends on both light pollution and lunar phase during observations. Detection limits of the 3.6-meter DOT at optical and NIR wavelengths are therefore estimated from observations taken on different epochs as described below.

5. Observations at optical wavelengths

Since March 2017, both point and extended celestial objects were imaged at optical wavelengths with IMAGER and ADFOSC mounted at the main axial port of 3.6-meter DOT (see Table 1). A brief description of these observations is given below.

The B, V and R broadband images of the galactic globular cluster NGC 4147 were obtained on six nights during 23 March 2017 to 9 April 2017. The sky brightness values estimated from the images taken on 23 March 2017 (dark night) are 22.29 ± 0.34 and 19.36 ± 0.21 mag/arcsec^2 in B and R bands respectively. These observations detect stars of B =24.5 mag and $R = 23.5$ mag with S/N ratio of 5 in the deep-colour magnitude diagram presented by Pandey *et al.* (2018). The numbers of short-exposure images ranging from 30 to 50 s taken in V and R bands were 339 and 302 respectively (see Lata *et al.* 2019). The FWHM values of these images ranged from 0.″7 to 1.″0. Based on these observations, Lata *et al.* (2019) identified and studied properties of 42 (including 28 newly discovered) periodic stellar variables.

A few optical transient sources were observed with IMAGER. A short-duration GRB 130603B afterglow and its host galaxy were imaged 1387 days after the GRB event. The flux values estimated from these observations have been used to construct the multi-wavelength spectral energy distribution of the host galaxy, which indicates that the host galaxy is young and blue with moderate values of star-formation activities (Pandey *et al.* 2019). Kumar *et al.* (2020) reported broadband optical photometric observations of the GRB 200412B afterglow taken with IMAGER during 15 to 25 April 2020. Multiple CCD frames, each with exposure time of 360 s, were taken in I, R and g bands. The GRB 200412B afterglow decayed $\sim$3 mag during the period of these observations. The magnitudes reported by Kumar *et al.* (2020) are listed in Table along with other relevant information. Detailed analysis of these data is in progress. The type II supernova (SN) ASASSN-16ab / SN 2016B located in the galaxy PGC 037392 was observed 465 days after its explosion, in 2 × 2 binning mode of IMAGER (Dastidar *et al.* 2019).

Using ADFOSC, optical observations of a GMRT high-redshift ($z \sim 4.8 \pm 2$) radio galaxy source (TGSS J1054 + 5832) were obtained on a dark night in SDSS r and i passbands. A statistically significant optical detection has been made in the i band (Omar *et al.* 2019b). The magnitudes and associated errors of this object as well as sky brightness derived from these observations are listed in Table 1. In i band imaging of the Abell cluster with ADFOSC, a source of 25 ± 0.3 mag has been detected by Omar *et al.* (2019a, c) in an exposure time of $\sim$1 hour. Sanwal *et al.* (2020) observed GRB 200524A optical afterglow on 24 May 2020 with ADFOSC. Several images of 300 s exposure time were taken in g, r and i bands. They clearly detect the optical transient and its r band magnitude is listed in Table 1. Further processing of the data is in progress.

The night sky brightness values at Devasthal are found to be 22.29 ± 0.34 and 19.36 ± 0.21 mag/arcsec^2 in the B and R photometric passbands respectively while they are $\sim$21 and $\sim$20.4 mag/arcsec^2 in the SDSS r and i bands respectively (Table 1). These numbers indicate that the night sky at Devasthal is dark in the optical region. The magnitude and associated error derived in different

Table 1. The back-end instruments used for optical and NIR observations of objects are given in the first and second column. Epoch, exposure time and filter used for observations are given in the third, fourth and fifth columns. The value of full-width half maximum (FWHM) in the sixth column was estimated from stellar images. Sky brightness and magnitude of the object derived from the observations are given in the last two columns along with their associated error.

Instrument	Object(s)	Epoch	Exposure (s)	Filter	FWHM ($''$)	Sky brightness (mag/arcsec^2)	Magnitude (mag)
IMAGER	NGC 4147	23 Mar 2017	1200	*B*	1.2	22.29 ± 0.34	24.5 ± 0.2
IMAGER	GRB 130603B	24 Mar 2017	600	*B*			22.13 ± 0.05
IMAGER	NGC 4147	23 Mar 2017	1200	*R*	1.12	19.36 ± 0.21	23.5 ± 0.2
IMAGER	GRB 130603B	24 Mar 2017	600	*R*			20.72 ± 0.02
IMAGER	SN 2016B	2 Apr 2017		*R*			19.79 ± 0.05
IMAGER	GRB 200412B	23 Apr 2020	4320	*R*	∼0.8		24.6 ± 0.12
IMAGER	GRB 200412B	24 Apr 2020	3600	*g*	∼0.9		25.2 ± 0.1
ADFOSC	TGSS J1054+5832	16 Apr 2018	3600	*r*	1.0	20.96 ± 0.2	24.5 ± 0.2
ADFOSC	TGSS J1054+5832	16 Apr 2018	3600	*i*	1.0	20.43 ± 0.2	24.9 ± 0.2
ADFOSC	GRB 200524A	24 May 2020	300	*r*			21.1 ± 0.03
TIRCAM2	M 92	11-22 May 2017	550	J	∼0.8	16.4 ± 0.2	19.0 ± 0.1
TIRCAM2	M 92	11-22 May 2017	550	H	∼0.8	14.0 ± 0.2	18.8 ± 0.1
TIRCAM2	M 92	11-22 May 2017	1000	K	∼0.8	12.2 ± 0.2	18.0 ± 0.1
TIRCAM2	WISE sources	11-22 May 2017	25	nbL	∼0.8	3.0 ± 0.2	9.2 ± 0.3
TIRCAM2	Czernik 3	7 Oct 2017	500	J	∼0.6	16.3 ± 0.2	19.9 ± 0.1
TIRCAM2	Czernik 3	7 Oct 2017	500	H	∼0.6	13.9 ± 0.2	18.6 ± 0.1
TIRCAM2	Czernik 3	7 Oct 2017	1000	K	∼0.6	12.2 ± 0.2	18.2 ± 0.1
TIRCAM2	NGC 7027	13 Oct 2017		K	∼0.8		
TIRCAM2	BD +36° 3639	10 May 2018		K	∼0.6		
TIRCAM2	IRC-20156	18 May 2018		K	∼0.7		
TIRCAM2	SAO 98770	21 May 2018		K	∼0.7		

photometric passbands for various objects are listed in Table 1. These numbers agree fairly well with the corresponding simulated values given by Pandey *et al.* (2018) for IMAGER assuming values of 3600 s and 1.$''$1 for integration time and seeing respectively. Stars of $B = 24.5 \pm 0.2, R = 24.6 \pm 0.12$ and $g = 25.2 \pm 0.2$ mag have been detected in exposure times of 1200, 4320 and 3600 s respectively. In photometric imaging mode of ADFOSC, a distant galaxy of 24.3 ± 0.2 mag and point sources of 25 ± 0.3 mag have been detected in the SDSS *i* band in one hour of exposure time. These detected magnitudes in different filters are ∼4 mag fainter than the corresponding magnitudes determined from similar observations taken with the 104 cm Sampurnanand telescope of ARIES located at Manora Peak, Nainital (Sagar 2018). However, out of this 4 mag gain, only 2.78 mag can be attributed to the difference in aperture sizes of the telescopes. The remaining gain in the detection limit of the 3.6-meter DOT can be attributed to the dark sky and better seeing at Devasthal even after completion of the telescope and surrounding buildings.

6. Observations at NIR wavelengths

The magnitudes estimated from TIRCAM2 observations taken during 11 to 22 May 2017 and on 7 October 2017 are used to quantify capability of the 3.6-meter DOT at NIR wavelengths. The magnitudes derived from these observations are listed in Table 1 along with other relevant information. They show that stars up to ∼20, 18.8 and 18.2 mag can be detected with 10% photometric accuracy in the *J*, *H* and *K* bands respectively. The corresponding effective

exposure times are 500, 550 and 1000 s respectively. TIRCAM2 is also capable of detecting the *nbL* band sources brighter than $\sim$9.2 mag and strong ($\geq$0.4 Jy) PAH emitting sources like Sh 2-61. Further details of these observations and associated errors are discussed in Ojha *et al.* (2018), Baug *et al.* (2018) and Sharma *et al.* (2020) along with science results. Baug *et al.* (2018) estimated 16.4, 14.0, 12.2 and 3.0 mag/arcsec^2 as sky brightness in *J*, *H*, *K* and *nbL* bands respectively. Similar values of sky brightness were also observed on 7 October 2017 during observations of the open star cluster Czernik (see Table 1). The values of sky brightness at Devasthal are comparable with those observed at other observatories like Hanle (Prabhu 2014), Calar Alto Observatory (Sanchez *et al.* 2008) and Las Campanas Observatory (Sullivan & Simcoe 2012). At NIR wavelengths, Devasthal sky has been characterized for the first time. Because of its observational capability up to 3.59 μm, the TIRCAM2 camera is an extremely valuable instrument for observing those bright *nbL* and PAH sources which are saturated in the Spitzer Infrared Array Camera observations.

Anand *et al.* (2020) imaged two young planetary nebulae (PNe), namely NGC 7027 and BD +30°3639 in *J*, *H*, *K*, PAH and *nbL* filters of TIRCAM2. These observations provided not only angular measurements of scientifically significant morphological features but also showed emissions from warm dust and PAHs in the circumstellar shells of these young PNe. During these observations, the value of FWHM of a stellar image in *K* passband was derived as 0.″76 and 0.″62 on the nights of 13 October 2017 and 10 May 2018 respectively (see Table 1). Using the technique of lunar occultation for the first time on the 3.6-meter DOT, Richichi *et al.* (2020) carried out high-angular-resolution measurements of unresolved IRC-20156 and resolved SAO 98770 binary stars with TIRCAM2. Based on these unique observations, Richichi (2020) derived scientifically important astrophysical results. On both nights of observation (18 and 21 May 2018), the value of FWHM of a stellar image in *K* passband was 0.″7 (see Table 1).

For the first time, on 6 June 2020, 3.6-meter DOT successfully observed an event of stellar occultation by a planet in *H* passband of TIRCAM2. The star UCAC4 340-192403 was occulted by Pluto. The present observations are particularly important since occultations by Pluto to be seen from Earth are getting rarer due to the fact that the dwarf planet now moves away from densely populated stellar regions of the Milky Way. Present high-signal-to-noise-ratio observations obtained as part of a global campaign are being analyzed and will be compared with models of Pluto's atmosphere. A publication based on these detailed investigations is under preparation.

7. Summary and future outlook

The values of FWHM estimated from images of stellar sources are listed in Table 1. They are expected to be slightly more than the values of atmospheric seeing prevailing at the epoch of observations as contribution from other sources of telescope image degradation discussed earlier in Section 2 are minimized by use of AOS. Atmospheric seeing is λ dependent and varies as $\lambda^{-0.2}$ (refer Sagar *et al.* 2019b). One can therefore confidently state that, at Devasthal, sub-arcsec atmospheric seeing is routinely observed at visual wavelengths. The natural atmospheric seeing observed at the site about two decades ago (see Sagar *et al.* 2000, and references therein), during 1997 to 1999, has, therefore, not deteriorated even after completion of the telescope and surrounding buildings. It is mainly because of the precautions taken in the design and the structure of the telescope building and locating the telescope floor $\sim$11 meters above the ground (Sagar *et al.* 2019a). All these, coupled with use of low-thermal-mass material in the telescope building and installation of modern and complex ventilation facilities to keep temperature gradient between telescope and its surroundings to the minimum, have paid a rich dividend in the undeteriorated natural atmospheric seeing at Devasthal. The 3.6-meter DOT can, thus, provide sky images with sub-arcsec resolution at wavelengths ranging from optical to NIR for a good fraction of observing time.

Performance verification of the telescope carried out during 2015-2016 after its installation at Devasthal indicates that all specifications given at the time of placing the order for the telescope in 2007 have been met successfully. Its on-sky imaging performance reveals that the quality of its optics is excellent and capable of providing images of celestial bodies with sub-arcsec (up to 0.″4) resolutions. Observations taken with IMAGER show that stars of $B = 24.5 \pm 0.2, R = 24.6 \pm 0.12$ and $g = 25.2 \pm 0.2$ mag have been

detected in exposure time of 1200, 4320 and 3600 s respectively. In the photometric imaging mode of ADFOSC, a distant galaxy of 24.3 ± 0.2 mag and point sources of 25 ± 0.3 mag have been detected in the SDSS i band in one hour of exposure time. The NIR observations taken with TIRCAM2 show that stars up to $J = 20 \pm 0.1, H = 18.8 \pm 0.1$ and $K = 18.2 \pm 0.1$ mag can be detected in effective exposure time of 500, 550 and 1000 sec respectively. The TIRCAM2 is also capable of detecting the *nbL* band sources brighter than ~ 9.2 mag and strong (≥ 0.4 Jy) PAH emitting sources like Sh 2-61. At NIR wavelengths, Devasthal sky is now characterized with TIRCAM2 observations. Both TANSPEC and TIRCAM2 at the focal plane of the 3.6-meter DOT are very much suited for the search for low-mass and very-low-mass stellar populations (M dwarfs, brown dwarfs), strong mass-losing stars on the asymptotic giant branch like young PNe (Anand *et al.* 2020), and young stellar objects still in their proto-stellar envelopes.

The modern 3.6-meter DOT observing facilities can provide optical and NIR observations for a number of frontline galactic and extra-galactic astrophysical research problems, including optical follow-up of γ-ray, X-ray, UV and radio sources observed with facilities like GMRT, AstroSat, etc., and optical-transient objects like SN, afterglows of γ-ray bursts and gravitational waves, etc. These studies will ultimately contribute to our understanding of various types of elements of the Periodic Table created about 150 years ago in 1869 by the Russian chemist Dmitri Mendeleev which revolutionized chemistry.

It is well known that a telescope only collects photons while the throughput of back-end instruments built using latest cutting-edge technology defines the quality of scientific output coming from it. It is essential to build modern and complex back-end focal-plane instruments so that the full astronomical potential of the 3.6-meter DOT can be utilized. One such instrument, named Devasthal Optical Telescope Integral Field Spectrograph (DOTIFS), is being fabricated by the Inter-University Centre for Astronomy and Astrophysics, Pune. DOTIFS is a multi-object integral field spectrograph. ARIES has recently initiated a process for building a modern high-resolution ($\sim 60{,}000$) spectrograph equipped with the most sensitive CCD detectors to be mounted on the telescope (Sagar 2019b). Addition of these back-end instruments will significantly increase scientific output from the 3.6-meter DOT.

Acknowledgements

This article is based on the invited talk delivered during the '150 years of Periodic Table' conference organized by the Indian Institute of Astrophysics (IIA), Bengaluru, during 16 to 19 December 2019. Constructive comments provided by anonymous reviewer are very much appreciated. We are thankful to the staff of ARIES for their assistance during the observations with the telescope. One of us (Ram Sagar) thanks the National Academy of Sciences, India (NASI), Prayagraj, for the award of a NASI Honorary Scientist position; the Alexander von Humboldt Foundation, Germany, for the award of Group linkage long-term research program; and the Director, IIA, for hosting and providing infrastructural support during this work.

References

Anand, R. K. *et al.* 2020, J. Astrophys. Astron., 41, Art. ID. No. 27. https://doi.org/10.1007//s12036-020-09644-9
Baug, T. *et al.* 2018, J. Astron. Instrumentation, 7, 1850003, https://doi.org/10.1142/S2251171718500034
Dastidar, R. *et al.* 2019, Mon. Not. Roy. Astron. Soc., 486, 2850
Kumar, A. *et al.* 2020, GCN Circular No. 27653
Kumar, B. *et al.* 2018, Bull. Soc. Royal Sci. Liege, 87, 29
Lata, S. *et al.* 2019, Astron. J., 158, 158:51, https://doi.org/10.3847/1538-3881/ab22a6
Naik, M. B. *et al.* 2012, Bull. Astron. Soc. India, 40, 531
Ojha, D. K. *et al.* 2018, Bull. Soc. Royal Sci. Liege, 87, 58
Omar, A. *et al.* 2017, Curr. Sci., 113, 682, https://doi.org/10.18520/cs/v113/i04/682-685
Omar, A. *et al.* 2019a, Curr. Sci., 116, 1472, https://doi.org/10.18520/cs/v116/i9/1472-1478
Omar, A. *et al.* 2019b, J. Astrophys. Astron., 40, Art. ID. 9. https://doi.org/10.1007/s12036-019-9583-4
Omar, A. *et al.* 2019c, Bull. Soc. Royal Sci. Liege, 88, 31
Pandey, S. B. *et al.* 2018, Bull. Soc. Royal Sci. Liege, 87, 42
Pandey, S.B. *et al.* 2019, Mon. Not. Roy. Astron. Soc., 485, 5294
Prabhu, T.P. 2014, Proc. Indian National Sci. Academy, 80, 887, https://doi.org/10.16943/ptinsa/2014/v80i4/55174
Richichi, S. *et al.* 2020, Mon. Not. Roy. Astron. Soc., 498, 2263, https://doi.org/10.1093/mnras/staa2403/astro-ph/2008.03459
Sagar, R. 2017, Proc. Natl. Acad. Sci., India, Sect A, 87, 1, https://doi.org/10.1007/s40010-016-0287-8
Sagar, R. 2018, Bull. Soc. Royal Sci. Liege, 87, 391
Sagar, R. *et al.* 2000, Astron. Astrophys. Suppl., 144, 349
Sagar, R. *et al.* 2011, Curr. Sci., 101, 1020

Sagar, R. *et al.* 2019a, Curr. Sci., 117, 365, https://doi.org/10.18520/cs/v117/i3/365-381
Sagar, R. *et al.* 2019b, Bull. Soc. Royal Sci. Liege, 88, 70
Sanchez, S. F. *et al.* 2008, Pub. Astron. Soc. Pacific, 120, 1244
Sanwal, P. *et al.* 2020, GCN Circular No. 27803
Sharma, S. *et al.* 2020, Mon. Not. Roy. Astron. Soc., 498, 2309, https://doi.org/10.1093/mnras/staa2412/astro-ph/2008.04102
Stalin, C. S. *et al.* 2001, Bull. Aston. Soc. India, 29, 39
Sullivan, P. W, Simcoe, R. A. 2012, Pub. Astron. Soc. Pacific, 124, 1336
Surdej, J. *et al.* 2018, Bull. Soc. Royal Sci. Liege, 87, 68